HHS Public Access

Author manuscript

Proc SPIE Int Soc Opt Eng. Author manuscript; available in PMC 2019 June 06.

Published in final edited form as:

Proc SPIE Int Soc Opt Eng. 2017 October ; 10572: . doi:10.1117/12.2285217.

Bayesian automated cortical segmentation for neonatal MRI

Zane Chou[1,2,*], **Natacha Paquette**[1,*], **Bhavana Ganesh**[1,2], **Yalin Wang**[4], **Rafael Ceschin**[5], **Marvin D. Nelson**[6,7], **Luke Macyszyn**[3], **Bilwaj Gaonkar**[3], **Ashok Panigrahy**[1,5,**], and **Natasha Lepore**[1,2,**]

[1]CIBORG laboratory, Department of Radiology, Children's Hospital of Los Angeles, CA, USA

[2]Viterbi School of Engineering, University of Southern California, CA, USA

[3]School of Computing, Informatics, and Decision Systems Engineering, Arizona State University, Tempe, AZ, USA

[4]Department of Radiology, Children's Hospital of Pittsburgh UPMC, Pittsburgh, PA, USA

[5]Department of Radiology, Children's Hospital of Los Angeles, CA, USA

[6]Department of Radiology, Keck School of Medicine, University of Southern California, Los Angeles, CA, USA

[7]Department of Neurosurgery, University of California Los Angeles, CA, USA

Abstract

Several attempts have been made in the past few years to develop and implement an automated segmentation of neonatal brain structural MRI. However, accurate automated MRI segmentation remains challenging in this population because of the low signal-to-noise ratio, large partial volume effects and inter-individual anatomical variability of the neonatal brain. In this paper, we propose a learning method for segmenting the whole brain cortical grey matter on neonatal T2-weighted images. We trained our algorithm using a neonatal dataset composed of 3 full-term and 4 preterm infants scanned at term equivalent age. Our segmentation pipeline combines the FAST algorithm from the FSL library software and a Bayesian segmentation approach to create a threshold matrix that minimizes the error of mislabeling brain tissue types. Our method shows promising results with our pilot training set. In both preterm and full-term neonates, automated Bayesian segmentation generates a smoother and more consistent parcellation compared to FAST, while successfully removing the subcortical structure and cleaning the edges of the cortical grey matter. This method show promising refinement of the FAST segmentation by considerably reducing manual input and editing required from the user, and further improving reliability and processing time of neonatal MR images. Further improvement will include a larger dataset of training images acquired from different manufacturers.

*Equal contribution first authors

**Equal contribution senior authors

Keywords

Cortical grey matter (cGM); Unmyelinated white matter (uWM); Neonatal brain; Prematurity; Magnetic resonance imaging (MRI); Brain tissue segmentation

1. INTRODUCTION

The last months of pregnancy are particularly important for the development of the child's brain and the effects of premature birth on neurological development are considerable. In spite of significant increases in survival rates, infants born preterm of very low birth weight remains at risk for poor neurological and neurodevelopmental outcomes[1–5]. In recent years, advances in neuroimaging techniques and quantitative methods have significantly improved the assessment of typical or atypical brain growth and the detection of brain injuries associated with prematurity[6,7]. Brain parcellation, or segmentation, refers to the labeling of a brain image into discrete anatomical or functional regions. An increasing number of image analysis tools are available to help neurologists and radiologists identify atypical brain structures or injuries in older subjects[8–11]. However, to date very few methods are able to precisely identify and categorize these regions in neonates and young children. This is largely due to the immature brain having a different water and fat composition than the adult one. The unmyelinated white matter in neonates and young infants typically gives neonatal images inverted cortical grey matter (cGM) and unmyelinated white matter (uWM) relative intensities, resulting in a smaller contrast between these tissue types (low contrast-to-noise ratio) as well as large partial volume effects[12–14]. Because of this, and along with the high anatomical variability in neonatal brain development, clinicians and scientists still largely use manual segmentation of neonatal brain tissue to examine overall brain growth or a given structure of interest in this population. This process is extremely time-consuming, as complete brain tissues segmentation (cortical and subcortical GM and WM structures, and cerebrospinal fluid (CSF)) can take up to 100 hours per infant[12] and is subject to intra and inter-rater variabilities.

Several attempts have been made recently to develop and implement an automated segmentation adapted to the neonatal and infant population[12,15–17]. However, there is still a paucity in the standardization and availability of these methods to the scientific community and in the clinic. Furthermore, most of the commonly available segmentation methods use the same thresholds for the entire image to label each voxel according to different tissue types. These approaches often fail to consider the variation in contrast and intensity of a given brain tissue within different regions of the neonatal brain (i.e. anterior vs. posterior differential maturation rate is reflected by different intensity contrasts between cGM and uWM). Here, we aim to address the low contrast-to-noise ratio of the uWM and cGM and differential regional maturation rate of the neonate brain in developing an automated segmentation method of the cGM. We combine a commonly used Bayesian probabilistic segmentation algorithm along with manually segmented T2-weighted MR images of preterm and full-term born neonates to generate a learning algorithm adapted to the neonatal population.

2. METHODS

2.1 Neonatal data

Our training dataset consists of 3 full-term neonates and 4 preterm neonates retrospectively recruited with visually normal MRI scans. The inclusion criteria for our preterm subjects were the following: 1) prematurity (fewer than 37 gestational weeks at birth), and 2) visually normal scans on conventional MR imaging. Demographic information of the neonatal dataset can be found in Table 1. All subjects with visible brain injuries such as intraventricular hemorrhage stage III or IV and hydrocephaly were excluded from the analysis. T2-weighted MRIs were acquired using a dedicated neonatal head coil on a 3T Siemens scanner at the Children's Hospital of Pittsburgh using a coronal three-dimensional (3D) Fast (Turbo) Spin Echo sequence (Matrix = 256 × 256 in plane), Resolution = $0.7\times0.7\times0.7$ mm^3, TE/TR = 418 ms/3100 ms, Flip angle = 120°, field of view = 180 mm in plane). The study protocol was approved by the institutional review board of the Children's Hospital of Pittsburgh and Children's Hospital Los Angeles.

2.2 Preprocessing

Preprocessing of the T2-weighted images was performed using the FMRIB's software library (FSL) (www.fmrib.ox.ac.uk/fsl). All images were skull-stripped using the Brain Extraction Tool (BET)[18] with bias field correction to account for field inhomogeneities. FMRIB's Automated Segmentation Tool (FAST)[19] was used to provide initial partial volume estimations (PVEs) for the cGM. Additionally, each image in the training set was manually segmented for cGM by an expert in pediatric neurology and reviewed by a second expert in pediatric radiology using ITK-SNAP[20].

2.3 Segmentation pipeline

The Bayesian segmentation pipeline is displayed in Figure 1. One healthy full-term neonate (Subject TC_046) from the training set was aligned (rotated and translated) to a neonatal template image from JER lab[21,22] using a 6 parameters linear registration from the FMRIB's Linear Image Registration Tool (FLIRT)[23,24]. The aligned image served as the template for the rest of the segmentation pipeline, providing a standard space for all training and test volumes. All PVEs and manually performed segmentations were registered to the standard space using the transformation matrix obtained from a 9 parameters FLIRT registration of their respective T2-weighted images to the template (Figure 1A–D).

Registering a manual segmentation from the native space to the standard space results in a non-binary mask with values ranging between 0 and 1. A binary mask for the registered manual segmentation can be obtained by thresholding the file such that voxels with a value above the threshold are given a value of 1, and voxels with value below the threshold are given a value of 0. To obtain the binary masks used in the training phase, all non-binary manual segmentations were thresholded at 0.5, as this yielded the most consistent and reliable binary masks for our dataset. Binary masks obtained using different threshold values are illustrated in Figure 2.

FSL FAST's segmentation compares PVEs to a single threshold value to determine whether to include each voxel in the segmentation. This often results in an overly inclusive grey matter segmentation in infants, including subcortical grey matter, cerebellum and brainstem, uWM. To address this, we used a Bayesian approach which adjusts the probability of a voxel being included in the cGM segmentation based on its position in standard space. This is achieved by thresholding the PVE output values according to a variable threshold at each voxel in the standard space. The optimal threshold value for each voxel was determined by minimizing the error between the PVE (Figure 1B) and the manually segmented binary mask (Figure 1C) across all subjects in the training set. The training algorithm used to determine the optimal threshold values and the 3D threshold matrix is displayed in Figure 3. Once this matrix was trained, each voxel in the registered cGM PVEs from the testing set (Figure 1D) was compared to the corresponding voxel in the threshold matrix (Figure 4). To smoothen the edges and have a continuous structure representative of the cGM morphology, we combined the segmentation obtained from FAST and Bayesian approach, and used the k-Nearest Neighbor (kNN) technique[12] (Figure 1E). The kNN determine the inclusion of a given voxel in the segmentation based on the prior inclusion of its nearest k neighbors in a 3×3×3 cube around the voxel of interest. This technique is sensitive to the local structure of the segmentation and is optimized for the k value to give the resulting segmentation (Figure 1F) the best possible representation of the cortical morphology.

To compare the Bayesian and FAST segmentations performance to that of the manual segmentation, the Dice similarity coefficients (DSC) were calculated for both techniques according to equation 1:

$$DSC = \frac{2|A \cap B|}{|A| + |B|} \quad (1)$$

This coefficient indicates the degree of similarity, or agreement, between images A and B, where A is an automated segmentation (FAST alone or Bayesian) and B is the manually segmented binary mask. Resulting DSC values ranges from 0 to 1, with lower values indicating no or low similarity and higher values denoting perfect or high similarity between the images.

Because of the limited sample size, we used a leave-one-out cross-validation method[25,26] to evaluate the performance of the model. This method allows better usage of data to obtain a more realistic Dice score. Thus, training was performed using 6 of the 7 available images, and testing was performed using the remaining image. This was repeated with for all the images available in our dataset.

3. RESULTS

Figure 5 shows the FAST-only segmentation (Figure 5C), the FAST segmentation (white) with a Bayesian mask (red) (Figure 5D), the final segmentation output using the Bayesian technique and k-NN smoothing (Figure 5E), and the manual segmentation (binary mask) of the cGM (Figure 5F) performed on all the images of the training set. Dice similarity scores

between the three methods and the manually segmented binary mask of the cGM are shown in Table 2.

The Dice similarity score found when comparing the automated Bayesian segmentation to that of the manual segmentation show high similarity, suggesting that little or minimal editing is required from the user following the segmentation process. Further inspection of Figure 5 indicates that in both populations, the automated Bayesian segmentation generates a smoother and more continuous segmentation compared to the FAST segmentation. The Bayesian mask (Figure 5D) applied on the FAST segmentation allow for the removal of the subcortical structures, while also cleaning the outer and inner edges of the cGM. The resulting Bayesian segmentation, combined with the k-NN smoothing, gives a more representative segmentation of the cGM morphology, improving the continuity and smoothness of the cortical segmentation.

4. DISCUSSION

Given the high MRI sensitivity to patient movements and the inherent difficulty in having young children remaining still for the acquisition duration, neonatal brain images require faster acquisitions and usually show poor signal-to-noise ratio[27,28]. In addition, partial volume effect artifacts often occur due to the poor intensity contrast of the unmyelinated white matter and the grey matter, leading to the mislabel of all tissue type (most frequently, labelling the CSF at the cGM boundaries as unmyelinated WM or excessively thick cGM)[29]. By combining the manual segmentation of the cGM and the Bayesian automated segmentation, we proposed an automated segmentation of the cGM adapted to the preterm and full-term neonate populations. Our method uses partial volume estimates (PVE) of the T2-weighted images as prior. The learning algorithm then generates probabilistic thresholds for every voxel by minimizing the error between the manually segmented cGM and the thresholded PVE.

When combined with the nearest neighbor smoothing, the automated Bayesian segmentation achieved a high similarity score compared to the manual segmentations. It successfully removed subcortical and cerebellar areas that were previously included in the FAST-only segmentation, and more accurately matched the delineation of cGM in terms of continuity and smoothness. Our method shows promising results given our limited training set and the high inter-individual variability of brain developmental rate in the neonatal population. In full-term and preterm neonates, in which higher inter-individual variability and lower contrast-to-noise ratio are frequently observed, the Bayesian method results in a smoother and more continuous cGM segmentation. The contribution of the Bayesian method to the commonly used FSL FAST algorithm provide an accurate and reliable parcellation of the neonatal cortex, with little manual editing required from the user. Our technique might reduce significantly the manual editing required from the user, thus improving both processing time and inter/intra-rater reliability throughout the segmentation process.

In future work, we plan to include additional manually segmented scans as part of the training set, including T2-weighted images acquired from different manufacturers to improve the stability and reliability of the segmentation pipeline. We also plan to improve

this pipeline by combining T1 and T2 weighted images to allow for a better grey and white matter contrast estimation, and by implementing normalization of local variation in intensity. We will also apply this pipeline on a larger dataset of prematurely and full-term born neonates. This pipeline will allow us to test for significant differences in whole brain cortical volume and morphometry between full-term and preterm born infants. These differences are likely to underlie important cognitive and neurodevelopmental outcomes that are frequently observed in preterm born children such as attentional deficit disorder or language delays.

Acknowledgments

We thank the families from Children's Hospital of Pittsburgh UPMC for their participation. The authors are also grateful for the help of Justine Aziz and Amrita Sandhu with the manual cortical segmentations. This work was supported by NIH grants K23NS063371, NIH/NCRR/NCATS and SC CTSI grant UL1 RR031986 (AP), and a CIHR research fellowship (NP).

References

1. Volpe JJ. The Encephalopathy of Prematurity - Brain Injury and Impaired Brain Development Inextrably Intertwined. Semin. Pediatr. Neurol. 16(4):167–178.2009; [PubMed: 19945651]
2. Volpe, JJ. Neurology of the Newborn. Saunders, H, editor. Elsevier; Philadelphia: 2008.
3. Volpe JJ. Brain Injury in premature infants: a complex amalgam of destructive and developmental disturbances. Lancet Neurol. 8(1):110–124.2009; [PubMed: 19081519]
4. Chau V, Synnes A, Grunau RE, Poskitt KJ, Brant R, Miller SP. Abnormal brain maturation in preterm neonates associated with adverse developmental outcomes. Neurology. 81(24):2082–2089.2013; [PubMed: 24212394]
5. Counsell SJ, Edwards aD, Chew ATM, Anjari M, Dyet LE, Srinivasan L, Boardman JP, Allsop JM, Hajnal JV, et al. Specific relations between neurodevelopmental abilities and white matter microstructure in children born preterm. Brain. 131:3201–3208.2008; [PubMed: 18952670]
6. De Vries LS, Groenendaal F. Neuroimaging in the preterm infant. Ment. Retard. Dev. Disabil. Res. Rev. 8(4):273–280.2002; [PubMed: 12454903]
7. Ment, LR, Hirtz, D, Huppi, PS. Lancet Neurol. Vol. 8. Elsevier Ltd; 2009. Imaging biomarkers of outcome in the developing preterm brain; 1042–1055.
8. Dale AM, Fischl B, Sereno MI. Cortical Surface-Based Analysis: I. Segmentation and Surface Reconstruction. Neuroimage. 9(2):179–194.1999; [PubMed: 9931268]
9. Fischl B, Sereno MI, Dale AM. Cortical Surface-Based Analysis. Neuroimage. 9(2):195–207.1999; [PubMed: 9931269]
10. Yushkevich P, Piven J, Cody H, Ho S. User-guided level set segmentation of anatomical structures with ITK-SNAP. Neuroimage. 31(3):1116–1128.2006; [PubMed: 16545965]
11. Yushkevich PA, Zhang H, Gee JC. Continuous medial representation for anatomical structures. IEEE Trans Med Imaging. 25(12)2006/12/16:1547–1564.2006; [PubMed: 17167991]
12. Anbeek P, Išgum I, Van Kooij BJM, Mol CP, Kersbergen KJ, Groenendaal F, Viergever MA, De Vries LS, Benders MJNL. Automatic segmentation of eight tissue classes in neonatal brain MRI. PLoS One. 8(12):1–9.2013;
13. Counsell SJ, Maalouf EF, Fletcher AM, Duggan P, Battin M, Lewis HJ, Herlihy AH, Edwards AD, Bydder GM, et al. MR imaging assessment of myelination in the very preterm brain. Am. J. Neuroradiol. 23(5):872–881.2002; [PubMed: 12006296]
14. Sled JG, Nossin-Manor R. Quantitative MRI for studying neonatal brain development. Neuroradiology. 55(SUPPL. 2)2013;
15. Song Z, Awate SP, Licht D, Gee JC. Clinical Neonatal Brain MRI Segmentation and Intensity-based Markov Priors. Med. Image Comput. Comput. Interv. :883–890.2007

16. Makropoulos A, Gousias IS, Ledig C, Aljabar P, Serag A, Hajnal JV, Edwards AD, Counsell SJ, Rueckert D. Automatic whole brain MRI segmentation of the developing neonatal brain. IEEE Trans. Med. Imaging. 33(9):1818–1831.2014; [PubMed: 24816548]
17. Gousias IS, Hammers A, Counsell SJ, Srinivasan L, Rutherford MA, Heckemann RA, Hajnal JV, Rueckert D, Edwards AD. Magnetic Resonance Imaging of the Newborn Brain: Automatic Segmentation of Brain Images into 50 Anatomical Regions. PLoS One. 8(4)2013;
18. Smith SM. Fast robust automated brain extraction. Hum. Brain Mapp. 17(3):143–155.2002; [PubMed: 12391568]
19. Zhang Y, Brady M, Smith S. Segmentation of brain MR images through a hidden Markov random field model and the expectation-maximization algorithm. IEEE Trans. Med. Imaging. 20(1):45–57.2001; [PubMed: 11293691]
20. Yushkevich PA, Piven J, Hazlett HC, Smith RG, Ho S, Gee JC, Gerig G. User-guided 3D active contour segmentation of anatomical structures: significantly improved efficiency and reliability. Neuroimage. 31(3)2006/03/21:1116–1128.2006; [PubMed: 16545965]
21. Richards, JE, Xie, W. Brains for all the ages: Structural neurodevelopment in infants and children from a life-span perspective. In: Bensen, J, editor. Advances in Child Development and Behavior. 2015. 1–52.
22. Richards JE, Sanchez C, Phillips-Meek M, Xie W. A database of age-appropriate average MRI templates. Neuroimage. 124:1254–1259.2016; [PubMed: 25941089]
23. Jenkinson M, Smith S. A global optimisation method for robust affine registration of brain images. Med. Image Anal. 5(2):143–156.2001; [PubMed: 11516708]
24. Jenkinson M, Bannister P, Brady M, Smith S. Improved Methods for the Registration and Motion Correction of Brain Images. Neuroimage. 17:825–841.2002; [PubMed: 12377157]
25. Kohavi, R. A Study of Cross-Validation and Bootstrap for Accuracy Estimation and Model Selection; Appear. Int. Jt. Conf. Articial Intell; 1995. 1–7.
26. Seni G, Elder JF. Ensemble Methods in Data Mining: Improving Accuracy Through Combining Predictions. Synth. Lect. Data Min. Knowl. Discov. 2(1)2010;
27. Mewes AUJ, Huppi PS, Als H, Rybicki FJ, Inder TE, McAnulty GB, Mulkern RV, Robertson RL, Rivkin MJ, et al. Regional Brain Development in Serial Magnetic Resonance Imaging of Low-Risk Preterm Infants. Pediatrics. 118(1):23–33.2006; [PubMed: 16818545]
28. Dagia C, Ditchfield M. 3 T MRI in paediatrics: Challenges and clinical applications. Eur. J. Radiol. 68(2):309–319.2008; [PubMed: 18768276]
29. Xue H, Srinivasan L, Jiang S, Rutherford M, Edwards AD, Rueckert D, Hajnal JV. Automatic segmentation and reconstruction of the cortex from neonatal MRI. Neuroimage. 38(3):461–477.2007; [PubMed: 17888685]

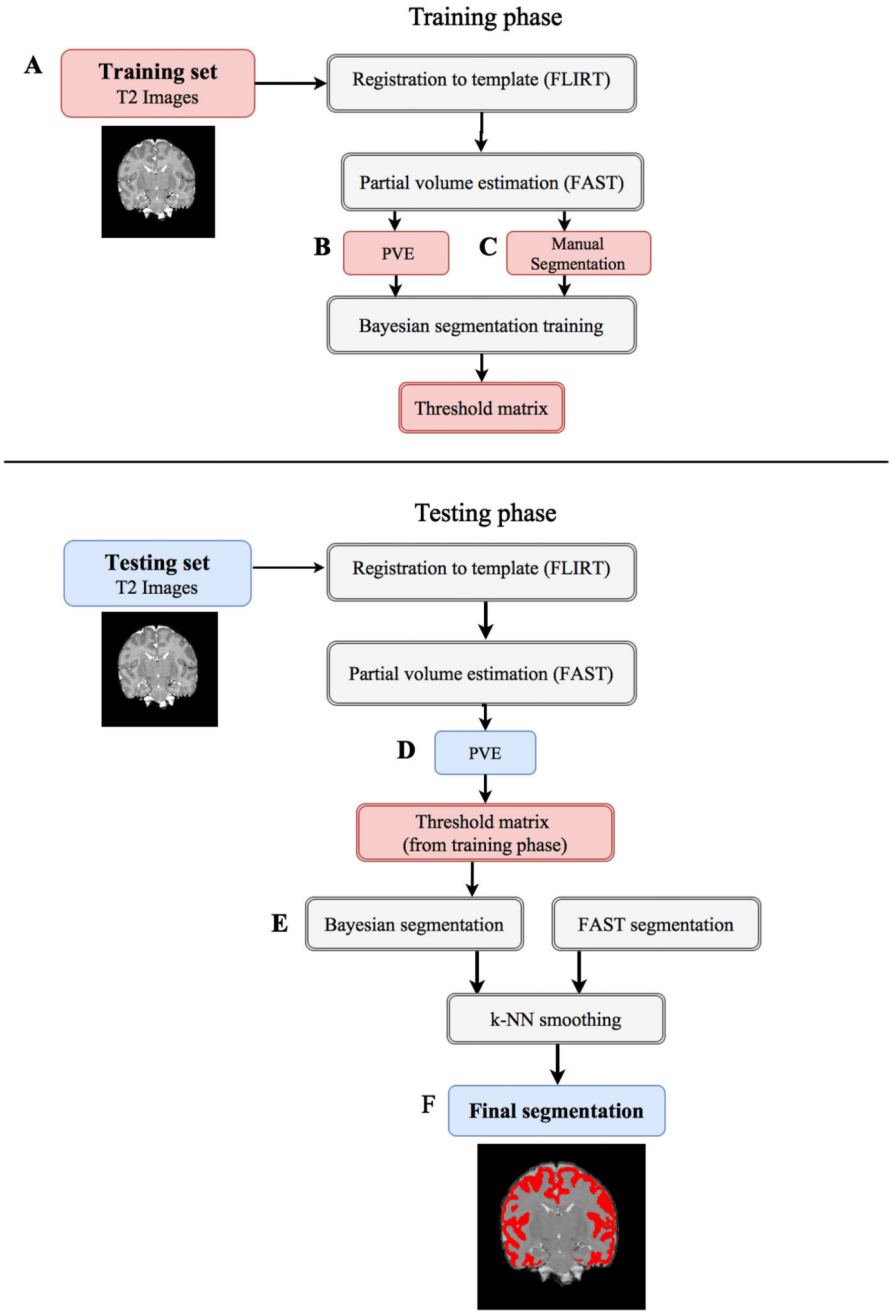

Figure 1.

The Bayesian segmentation pipeline. Training phase: After images registration to the standard template, a threshold matrix is created to find the optimal values that minimize the error between the partial volume estimations and manual segmentations from the training set images. Testing Phase: Automated segmentations are then obtained from comparing the registered PVE of target images with the threshold matrix values for each voxel in the template space. Details regarding the training algorithm used to determine the optimal threshold values can be found in Figure 3. For the final output, the binary results from FAST

and Bayesian cortical segmentation are combined and smoothened using the k-Nearest Neighbor (kNN) technique.

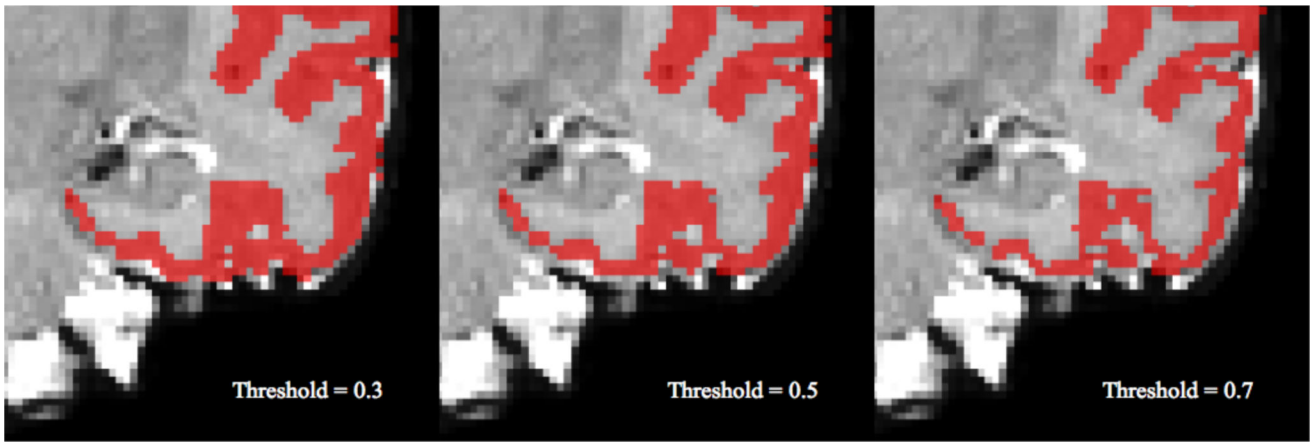

Figure 2.
The registered manual segmentation thresholded at 3 different values. Lower thresholds are overly permissive, while higher thresholds can leave breaks in the segmentation.

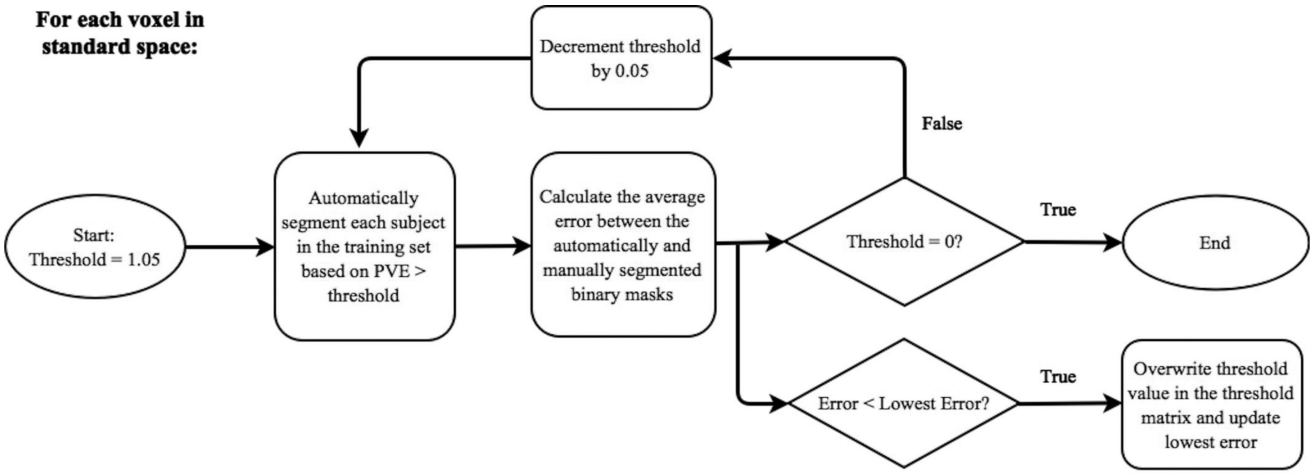

Figure 3.

Threshold training performed for each voxel in the common space. This algorithm determines the threshold value that minimizes the error between the automated and manual segmentations in the training set.

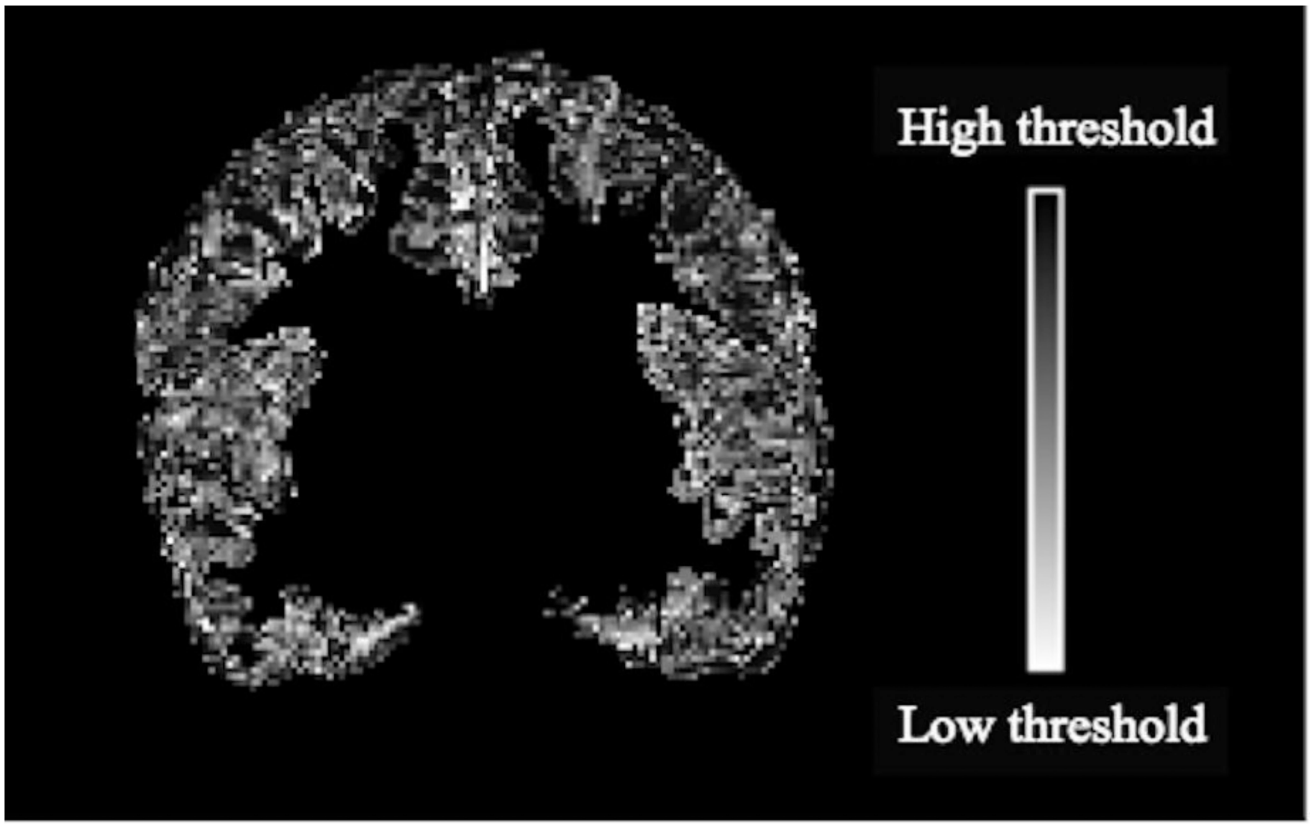

Figure 4.
The resulting matrix of optimal threshold values after the training phase. Voxels with higher thresholds require high PVE values to be included in the segmentation. Voxels with lower thresholds are included more readily. All PVE outputs in the testing phase are thresholded using this matrix.

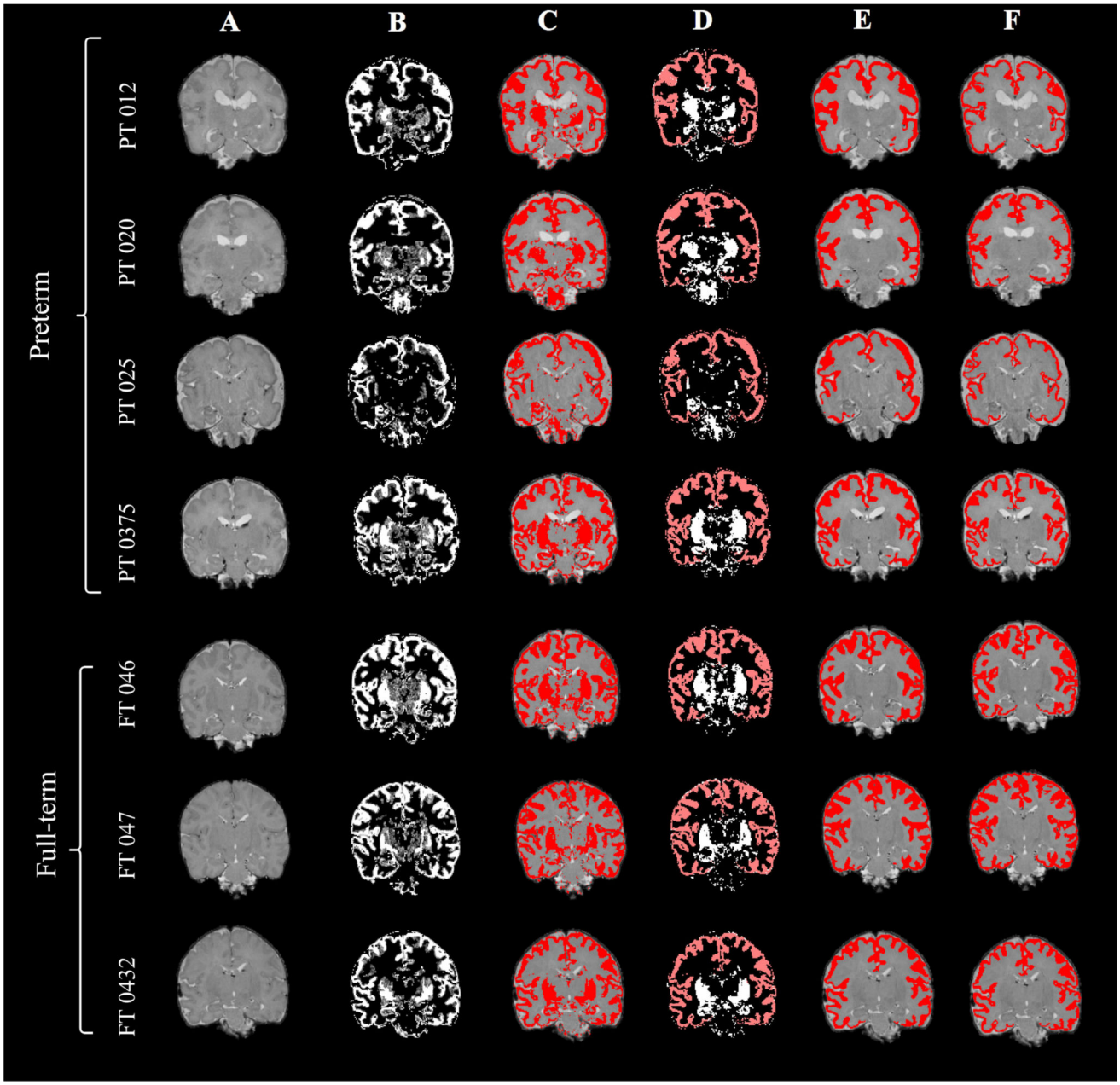

Figure 5.

Images for all subjects in the training set. A) Linearly registered T2-weighted MRI images. B) cGM partial volume estimation. C) FAST segmentation. D) FAST segmentation (white) with Bayesian mask (red) E) Final segmentation using Bayesian technique and k-NN smoothing F) Manual segmentation.

Table 1

Demographic and birth data

	Subject ID	Gender	Gest Age at birth (weeks)	Birth weight (g)	Gest Age at scan (weeks)	Apgar 1 min	Apgar 5 min
Preterm	012	M	31.9	1910	36	4	7
	020	F	29.1	1064	36	4	6
	025	M	37	2477	37	9	9
	0375	F	31.0	3290	38	8	9
Full-term	0432	M	37.0	3940	37	7	8
	046	F	37.1	2552	40	NA	NA
	047	M	39.1	3130	40	9	9

Table 2

Dice Similarity Coefficients comparing the performance of FAST only and FAST with Bayesian Segmentation to the manual segmentation of each subject.

	Subject ID	FAST only	FAST with Bayesian Segmentation
Preterm	012	0.6900	0.7888
	020	0.7665	0.8518
	025	0.6920	0.7684
	0375	0.7867	0.8638
Full-term	0432	0.8199	0.8865
	046	0.7816	0.8836
	047	0.8142	0.8799
Average		0.7644	0.8461